RGNZ/MGPB

Identifying the Basement Structure of the Sula Fault Zone in the Banggai-Sula Microcontinent Region, Molucca Sea, based on 2D Gravity Inversion Modelling using Particle Swarm Optimisation and 3D Modelling using Grablox

Rudarsko-geološko-naftni zbornik
(The Mining-Geology-Petroleum Engineering Bulletin)
UDC: 550.3; 550.8
DOI: 10.17794/rgn.2025.2.10

Original scientific paper

Cahya Damayanti[1,2]; Sismanto Sismanto[1]*; Ari Setiawan[1]; Lina Handayani[2]
[1]*Department of Physics, Gadjah Mada University, Yogyakarta 55281, Indonesia*
[2]*Research Center for Geological Disaster, National Research and Innovation Agency, Bandung 40135, Indonesia*

Abstract
This study aims to delineate the basement structure of Sula fault zones within the Banggai-Sula Microcontinent Region through the implementation of 2D and 3D gravity inversion modelling. The Sula fault is a consequence of the convergence between the Banggai-Sula Microcontinent and northern regions, or the compression caused by the extrusion of material from the Molucca Sea collision zone to the south. This is an active fault, with a few earthquakes in the last two decades. As a complex active fault, this presents several questions, particularly about the fault's structure. Residual anomaly data was modelled in two dimensions using Particle Swarm Optimisation method and in three dimensions with Grablox software. The gravity inversion results indicate that the basement depth in the nine profile incision zones, which are perpendicular to the fault zone, range from 120 m to 9308 m. This research region can be separated into two fault zones based on the low-value residual anomalies. Fault zone 1 exhibits a basement depth range of 2843.3 m to 6526.9 m. This region has rock components with a low density ranging from 1.68 g/cm^3 to 2.20 g/cm^3. Fault zone 2 exhibits a basement depth range of 3716.3 m to 9308.4 m. The geological layer comprises constituent rocks with a low density of 1.24 g/cm^3, in contrast to the northern rocks averaging 2.4 g/cm^3 and the southern rocks averaging between 2.5 g/cm^3 and 2.7 g/cm^3.
The average depth of faults in fault zones 1 and 2 is 5200 m. The inversion method using PSO can yield estimates for the basement depth of the fault zone. Derivative analysis indicates that the east-west-trending fault structure in fault zone 1 and fault zone 2 aligns with the tectonic characteristics of the Banggai-Sula microcontinent, hence affirming the presence of an east-west fault in the area.

Keywords:
gravity; inversion modelling; particle swarm optimisation; Banggai-Sula; Molucca Sea

1. Introduction

The tectonic activity of the Indo-Australian Plate, Pacific Plate, and Eurasian Plate around Sulawesi Island has significantly influenced tectonic changes in Sulawesi and its vicinity (**Hall, 2002; Hamilton, 1979**). The Mesozoic era, marked by the growth of Australia's northwestern shelf, initiated this process. This, in turn, led to the fragmentation of the Australian Continent's edge, resulting in the formation of multiple microcontinents, including the Banggai-Sula Microcontinent (**Zakaria and Sidarto, 2015**). The westward displacement of the Banggai-Sula Microcontinent was impeded by its collision with the East Arm of Sulawesi, the dating of which remains contentious (**Ferdian et al., 2011; McCaffrey et al., 1980; Watkinson et al., 2011**).

In the northern region of the Banggai-Sula microcontinent, a segment of the Sula rising fault is present. The Sula thrust is typically depicted as a significant structure aligned with the northern boundary of the Sula platform (**Garrard et al., 1988; McCaffrey et al., 1980; Silver et al., 1983**). The Sula thrust is a consequence of the convergence between the Banggai-Sula Microcontinent and northern regions, or the compression caused by the extrusion of material from the Molucca Sea collision zone to the south (**Pigram and Supandjono, 1985**). This is an active fault, with a few earthquakes in the last two decades (see **Figure 1**). As a complex active fault, this presents several questions, particularly regarding the fault's structure. According to multibeam data, there is no evidence of a continuous E-W-running North Sula-Sorong fault as depicted on numerous maps (**Ferdian et al., 2011**). The current study primarily concentrates on clarifying the tectonic evolution of the collisional orogen in Sulawesi and the western extremity of the Banggai Sula Microcontinent. However, the northern boundary of the Banggai-Sula Microcontinent has received little attention, especially when it comes to the structure of the Sula thrust fault in this region (**Watkinson et al., 2011**). This research aims to delineate the basement structure of the northern region of the Banggai-Sula Microcontinent, with particular emphasis on the Sula fault in the Molucca Sea (see **Figure 1**).

* Corresponding author: Sismanto Sismanto
e-mail address: sismanto@ugm.ac.id

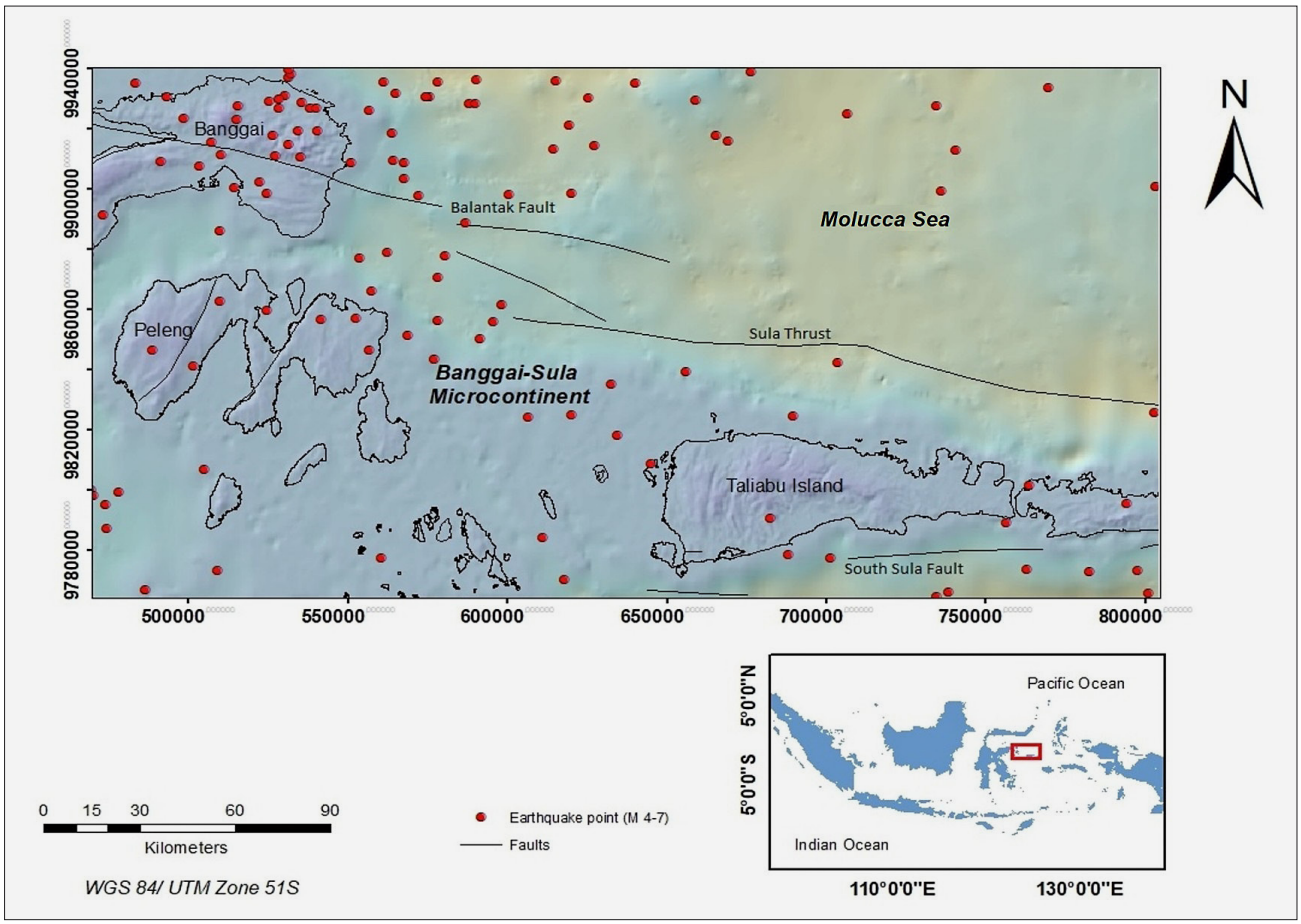

Figure 1: Bathymetric map of the study area with an inset indicating the research location (the source of the faults line refers to the Indonesian earthquake source and hazard map (**PuSGeN, 2017**)).

We use gravity data from Topex satellite observations to create a two-dimensional representation of the fault foundation structure in the study area. We adjusted satellite-derived gravity anomaly data for free-air correction, further processed it to derive terrain adjustments, and ultimately used it to create Complete Bouguer Anomaly (CBA) data (**Maulana et al., 2021**). The complete Bouguer anomaly data consists of total gravity anomaly data, reflecting the entire subsurface geological framework.

All common methods, whether geophysical or geological, on land or at sea, may effectively map underlying structures. Conversely, it necessitates substantial time and financial resources, as well as the involvement of numerous individuals in data collection. Researchers have developed geophysical methods of collecting data using satellite technology, as well as field methodologies that directly collect data in the studied area. One example of such a data source is pertaining to gravitational anomalies. An example of the gravity method utilizing satellite altimetry data is to analyse basin features off the coast of Central Sulawesi (**Setiadi et al., 2021**). A regional study of gravity anomalies in the Southeast China Sea explored the inversion method in analysis (**Zhang et al., 2017**). The gravity method has been regarded as a highly effective geophysical technique for illustrating underlying features. Satellite data has been very commonly used to characterise gravity anomalies in marine regions to assess sea floor depth (**Smith et al., 1997**).

For the inversion approach, the Particle Swarm Optimisation (PSO) is a robust stochastic optimisation method and one of the most often utilised global optimisation methods, owing to its minimal control parameter needs and straightforward implementation (**Alqahtani et al., 2022**). A study by **Roy et al. (2021)** used global optimisation techniques and Particle Swarm Optimisation (PSO) to figure out the depth of different sedimentary basins in India's Godavari basin and Mexico's Sayula basin by looking at the vertical components of residual gravity anomalies. The previous publications (**Chakravarthi, 2005; Rao, 1990**) detailed the equations for inversion issues in gravity based on various density models. The exponential depth density variation model was proposed in **Chapell and Kusznir (2008); Cordell (1973);** and **Granser (1987)**. Gravity inversion using Particle Swarm Optimisation (PSO) to determine basement depth was introduced in **Alqahtani et al. (2022); Pallero at al. (2015, 2021); Toushmalani (2013)**. The analysis of satellite gravity data has demonstrated considerable efficacy in preliminary sub-surface geological

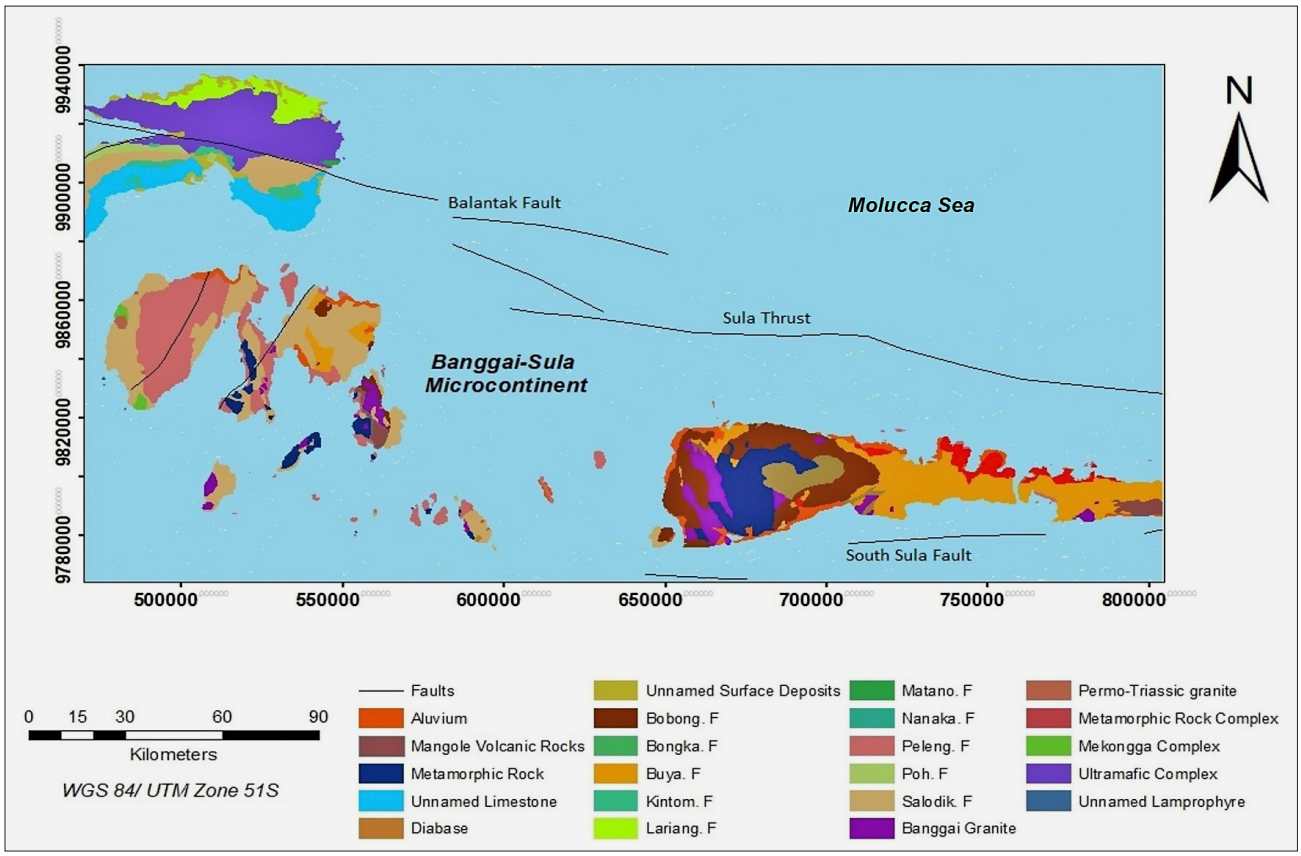

Figure 2: Geological map of the research area
(modified from **Supandjono and Haryono, 1993; Surono and Sukarna, 1993**).

mapping in some inaccessible regions. Global optimisation methods, when applied to the PSO algorithm for density contrast estimation, have yielded effective results. At the same time, the field of research on basement depth and structural geology in fault zones based on gravity data is still relatively unexplored. This research seeks to ascertain the depth of the basement and delineate the geometry of subsurface structures inside the fault zone, particularly the Sula fault, utilising 2D and 3D gravity inversion optimised by the PSO method (**Pallero et al., 2021**) for enhanced clarity.

2. Geology of the Research Area

The eastern arm of Sulawesi comprises multiple geological formations, including the Bobong, Kintom, Lariang, Nanaka, Poh, Bongka, and Matano formations (**Garrard et al., 1988; Pigram and Supandjono, 1985; Surono, 2012**). Besides the previously mentioned formations, this region also features ultramafic complexes and an unidentified limestone (see **Figure 2**). The study area is located in the Banggai-Sula Microcontinent, west of Molucca Sea. The predominant rocks include metamorphic, volcanic, and granite formations from the Paleozoic to Triassic periods. Clastic and carbonate deposits from the Jurassic-Cretaceous period cover these three rock types. The earliest rocks are metamorphic, comprising schist, mica schist, gneiss, phyllite, metamorphic sandstone, and argillite from the Carboniferous period. Additionally, they deposited Mangole volcanic rocks, which are believed to be of Permo-Triassic age. The materials comprise eroded tuff, ignimbrite, lapilli tuff, and volcanic breccia. Granite plutons from the Permo-Triassic period have intruded the metamorphic rock. We refer to the granite located here as Banggai granite. Metamorphic and volcanic rocks serve as the foundational source of subsequently deposited rock units. The Nofaini limestone unconformably overlies bedrock composed of crystalline and coralline limestone, believed to be of Triassic age. The Bobong Formation, the Buya Formation, and the Tanamu Formation overlay unconformable bedrock. The Bobong Formation has interbedded conglomerate, sandstone, and shale, together with coal, believed to date from the Early to Middle Jurassic period. The Buya Formation dates to the Middle Jurassic period. The Late Jurassic comprises shale interspersed with sandstone, limestone, marl, and conglomerate. Minor intrusions of volcanic rock, consisting of basalt and diabase, penetrate the foundational layers of the Kabau Formation and Buya Formation. Above the Buya Formation lies the Late Cretaceous Tanamu Formation. The geological formations comprise marble, calcareous limestone, and shale. The Salodik Formation, dating to the early-to-mid Miocene epoch, unconformably succeeds

the Tanamu Formation. The formation comprises limestone interspersed with sandstone (**Garrard et al., 1988; Saultan and Subagio, 2014**).

Silver et al. (1983) identified the Sula Thrust, a continuous northward-dipping impact zone, south of the Sula-North Sorong Fault. The Sangihe and Halmahera faults, located above the double subduction zone in the Molucca Sea, predominantly manage approximately 10 cm/a of convergence between the Philippine Sea and the Eurasian Plate north of the Sula–North Sorong fault (**McCaffrey et al. 1980; Moore and Silver 1980**). The southward compression of sediments within this zone led to the formation of the Molucca Sea collision complex (**Silver et al., 1983). Hamilton (1979)** identified The South Sula fault as traversing the southern slope of Taliabu and situated between Mangole and Sanana. The large rise in water depth south of this line shows that oceanic crust is under the area. This is supported by crustal and marine geophysical data from the North Banda basin. The fault then marks the southern limit of the Banggai-Sula Microcontinent. The South Sula fault is a horizontal fault extending eastward to Irian Jaya, believed to have facilitated the left-lateral translation of the Banggai Sula Microcontinent (**Beaudouin et al., 2003**).

3. Methods

3.1. Data acquisition and data processing

This research pertains to the Banggai-Sula Microcontinent, situated within the Molucca Sea and the eastern extension of Sulawesi Island, at coordinates 0° 32'–2° 16' N latitude and 122° 31'–123° 53' E longitude (see **Figure 1**). We acquire free air anomaly data from the Topex website (http://Topex.ucsd.edu/cgi-bin/get data.cgi). The mass above the Earth's surface affects this anomaly, requiring a topographic correction that includes the Bouguer correction (**Blakely, 1996**). This work applied the Bouguer adjustment to two regions: the marine area and the terrestrial area. For marine regions the corrections can be implemented after we established the density and depth of the water. In marine environments, we can conceptualize the Bouguer correction as an endless slab that corresponds to the water depth and has a density equal to the difference between water and rock (**Lillie, 1999**). The formula for determining the Bouguer anomaly value in marine regions is outlined in **Equation 1** and **2**.

$$BCs = (0.0419)\rho(H - h) = \\ = 0.0419(\rho_w - \rho_c)h_w \quad (1)$$

$$\Delta g_{Bs} = \Delta gfa + BCs \quad (2)$$

where:

BCs – the Bouguer correction at marine area (mGal),
h_w – the water depth from the observation site (m),
ρ_w – the density of seawater is (1.03 g/cm³),
ρ_c – the density of seabed rocks is (2.67 g/cm³),
Δg_{Bs} – the Bouguer anomaly at sea(mGal).

The slab's thickness corresponds to the sea's depth (**Lilie, 1999**).

For the terrestrial area, the Bouguer gravity anomaly (Δg_B) is derived by removing the influence of the infinite slab (BC) from free air gravity anomalies. The formula for determining the Bouguer anomaly value in above sea level regions is outlined in **Equation 3** and **4**.

$$BC = (0{,}0419)\rho H \quad (3)$$

$$\Delta g_B = \Delta gfa - BC \quad (4)$$

where:

BC – the Bouguer correction (mGal),
ρ – the density of rocks (g/cm³),
H – elevation (m),
Δg_B – the Bouguer anomaly (mGal),
Δgfa – free air anomaly (mGal).

The previously described infinite Bouguer slab correction yields a straightforward Bouguer anomaly. This correction is typically adequate for estimating masses above the datum or sea level in regions where the topography closely resembles the slab. However, in irregular terrains, the proximity of mountains may exert a substantial upward gravitational influence on the station, or valleys devoid of mass, resulting in an absence of gravitational force. For such circumstances, it is important to apply Terrain Correction (TC), which is then added to the simple Bouguer anomaly (Δg_B), thus producing a complete Bouguer gravity anomaly (Δg_{BC}), as depicted in **Equation 5**. We then processed the terrain correction data to derive the Complete Bouguer Anomaly (CBA), as shown in **Figure 3**.

$$\Delta g_{BC} = \Delta g_B + TC \quad (5)$$

The distribution map of the Complete Bouguer Anomaly (CBA) in **Figure 3** indicates that the anomalies range from -47.9 mGal to 297.8 mGal. The entire Bouguer anomaly map indicates that regions with low CBA values are located in the northern section, specifically in the Molucca Sea and portions of the eastern arm of Sulawesi. The regions exhibiting elevated CBA values are located in the southeastern section of the research area, specifically inside the Banggai islands and Taliabu Island. The elevated Bouguer anomaly indicates the existence of dense rocks, such as oceanic crust, near the surface. This is directly associated with the Sula fault, which traverses from west to east at this site.

This research focuses on the residual anomaly depicted in **Figure 4**, necessitating the separation of complete Bouguer anomaly data from gravitational influences attributed to regional anomalies. This research employed the Radially Averaged Power Spectrum (RAPS) curve analysis method, utilising a bandpass filter to separate gravity anomalies (**Gunawan et al., 2022**).

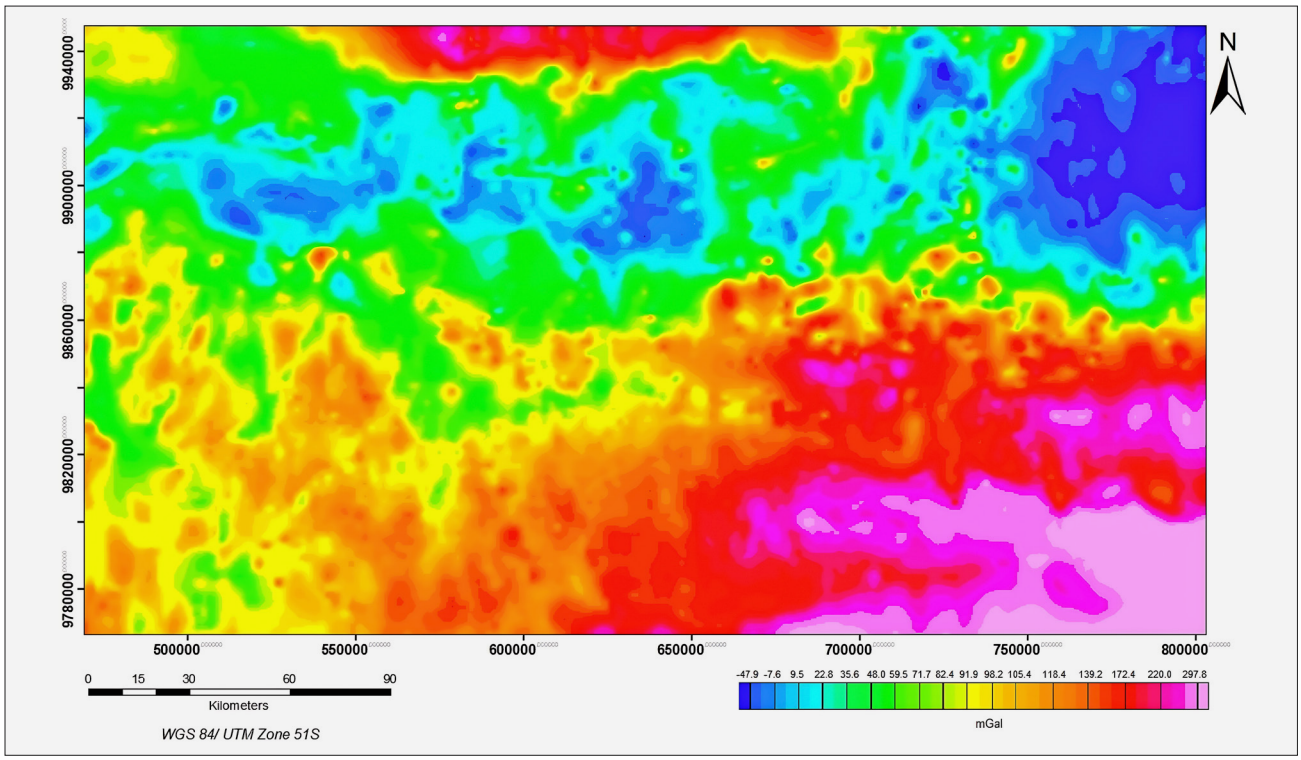

Figure 3: The research area's complete Bouguer anomaly map displays the highest Bouguer anomaly value in the purple region

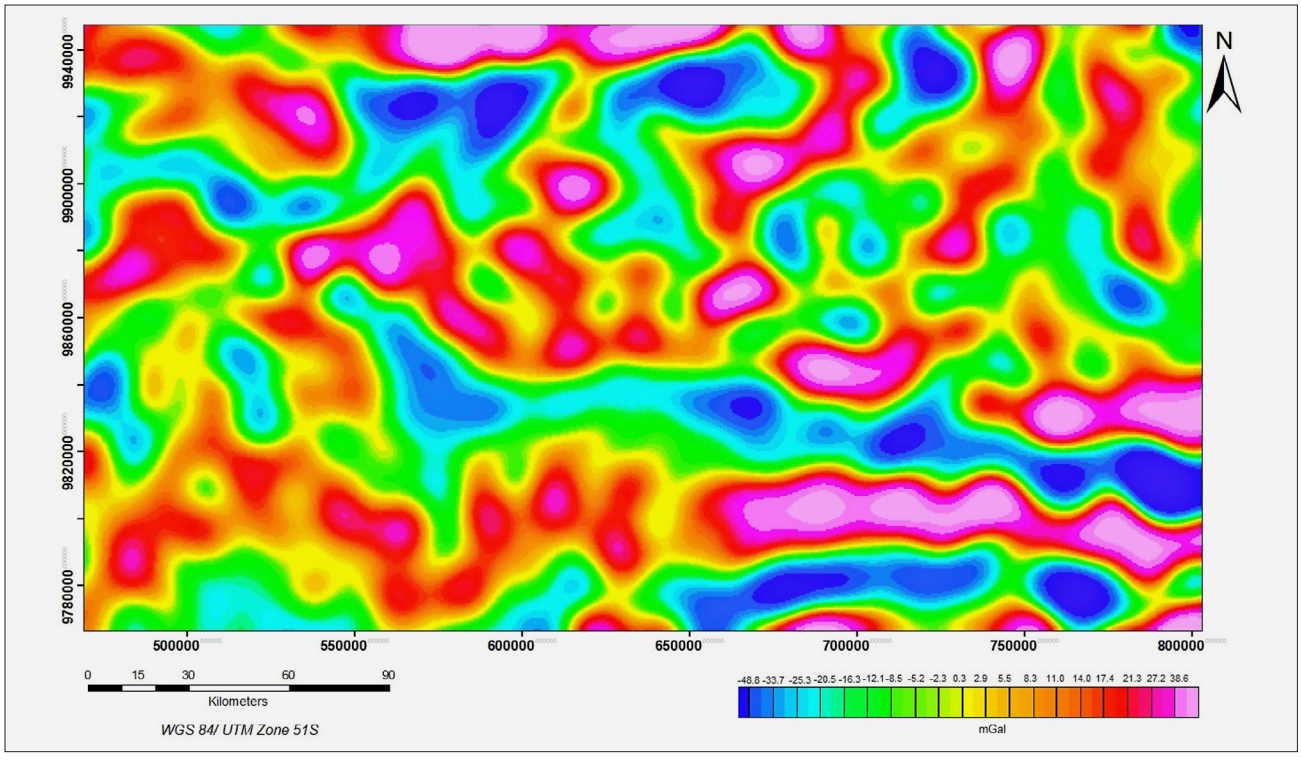

Figure 4: A residual anomaly map of the study area, derived from the CBA separation of regional influences. A persistent high anomaly in purple signifies the existence of rocks with elevated density values.

Figure 4 shows the residual anomalies. Residual anomalies identify anomalous source rocks located at shallow depths and exhibit a high frequency. The distribution of residual anomalies in the studied area exhibits gravity anomaly values between -48.8 mGal and 38.6 mGal. Upon isolating the anomalies, the distribution of residual anomaly values generally exhibits a lesser magnitude than that of the complete Bouguer anomaly. The

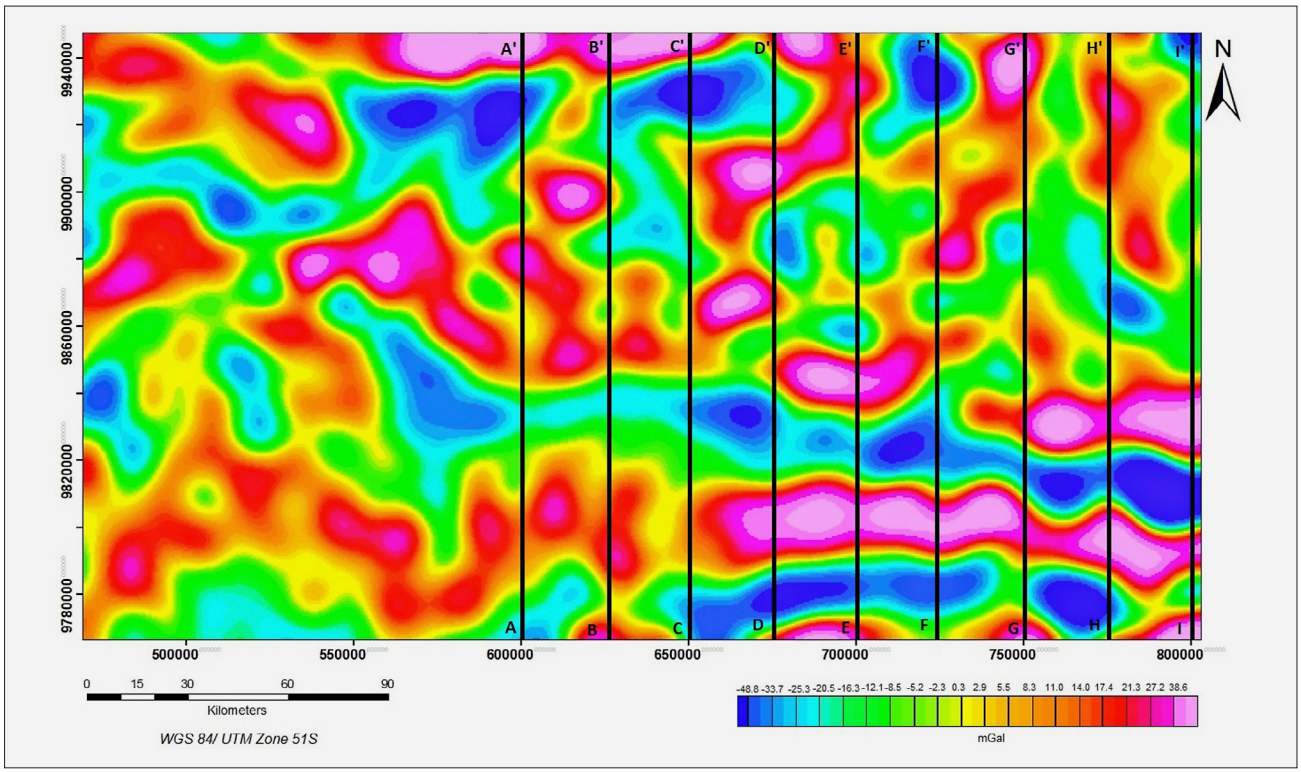

Figure 5: The residual map shows nine profile cuts oriented south-north intersecting perpendicularly with the Sula fault zones, which align generally east-west.

distribution of low residual anomalies ranges from -48.8 mGal to -2.3 mGal, depicted in blue to yellowish green. The distribution of low anomalies generally exhibits a negative value, which is prevalent throughout the studied area. Orange to purple indicate anomalies with values ranging from 8.3 mGal to 38.6 mGal, indicating elevated rock density.

3.2. Horizontal derivative analysis

We used horizontal derivative analysis to define anomaly boundaries for superficial gravity anomaly sources. The gravitational anomaly value changes between two points at a certain distance in this study. This is calculated using the first order FHD (First Horizontal Derivative) and the second order SHD (Second Horizontal Derivative). We computed the FHD value by determining the gradient between the two nearest gravitational field data points, $g\ (r_1)$ and $g\ (r_2)$, and express the horizontal component values as x and r in the following formula.

$$\left|\frac{dg}{dr}\right| \approx \left|\frac{\left[g(r_1)-g(r_2)\right]}{\Delta r}\right| \tag{6}$$

To ensure that the orientation of the gravitational field data points does not affect the FHD calculation procedure, we employed the absolute value in **Equation 6** (**Rosid and Siregar, 2017**). The SHD value was determined by calculating the gradient between the two nearest FHD data points, as defined below:

$$\left|\frac{d^2\Delta g}{dr^2}\right| = \left|\frac{\left[\frac{dg(r_2)}{dr}-\frac{dg(r_1)}{dr}\right]}{\Delta r}\right| \tag{7}$$

The results derived by FHD analysis represent the maximum and minimum values at the interface of abnormal items. A zero value in the second-order derivative may signify the existence of structural boundaries in the gravity data.

This research involves derivative analysis utilising residual map data with nine vertical profile incisions oriented south to north, as illustrated in **Figure 5**. We evaluated multiple factors prior to establishing the orientation of the 2D cross-sectional profile incision. The orientation and distribution of trending faults are predominantly east-west, in line with the topography of the study area.

These nine profile incisions are spread perpendicularly in the Sula fault area, with the path length of each profile incision A-A', B-B', C-C', D-D', E-E', F-F', G-G', H-H', and I-I' being 181,416.85 meters. We conducted derivative analysis in first order (FHD) and second order (SHD). Upon exceeding the subsurface structure density contrast threshold, the first-order horizontal derivative will exhibit either a maximum or minimum value, but the second-order horizontal derivative will display a zero value (**Cordel, 1973**).

3.3. Particle Swarm Optimisation (PSO)

Particle Swarm Optimisation (PSO) is a stochastic evolutionary computation method (**Eberhart and Kennedy, 1995**) that has been effectively applied across various engineering disciplines. Our study applied the method proposed by **Pallero et al. (2015)** for gravity inversion. The PSO method was inspired by the social behaviour of individuals, termed particles, found in nature, such as flocks of birds and schools of fish. This method emulates the behaviour of a flock of birds randomly searching for a singular food source inside a designated area. Not all birds possess knowledge of the precise location of food; they merely discern the distance to it during each search. He subsequently employed the bird gathering scenario to address optimisation concerns. Each particle adjusts to its optimal position, referred to as p_{best}, based on its fitness value (**Cholissodin and Riyandani, 2016**). A particle that adopts the optimal position of the entire population, determined by comparing the best fitness values of all particles in the swarm, is referred to as g_{best} or the global best position during the exploration of the search space (**Cholissodin and Riyandani, 2016; Mohapatra, 2013**). Through p_{best} and g_{best}, the particles regenerate to create the subsequent generation of the swarm.

On every particle p can be represented via an n-dimensional vector: the first vector is defined as:

$C_p^k = \left(C_{p1}^k, C_{p2}^k, \ldots, C_{pn}^k\right)$, with $p = (1,2,...,pn)$ which shows the position of the particle p in the search space on iteration k.

The second vector is written $V_p^k = \left(V_{p1}^k, V_{p2}^k, \ldots, V_{pn}^k\right)$ which represents the speed of particle movement p.

The third vector is written $P_{best_p}^k = \left(P_{best_{p1}}^k, P_{best_{p2}}^k, \ldots, P_{best_{pn}}^k\right)$ shows the best position of the third particle p and the final vector is written $G_{best_p}^k = \left(G_{best_{p1}}^k, G_{best_{p2}}^k, \ldots, G_{best_{pn}}^k\right)$ which represents the global best position in the swarm until the th iteration – k. The flock is updated by the following **Equation 8** (**Xu et al., 2015**).

$$V_{pn}^{k+1} = \theta V_{pn}^k + b \times rand1(b)\left(P_{best_{pn}}^k - x_{pn}^k\right) + \\ + c \times rand2(c)\left(G_{best_{pn}}^k - x_{pn}^k\right);$$

$$C_{pn}^{k+1} = C_{pn}^k + V_{pn}^{k+1} \quad (8)$$

where:

b and c – parameters

rand1(b) and rand2(c) – a random number that is uniformly distributed in the interval [0,1]

coefficients b and c – positive constants to control how far a particle will move in each iteration

i – the inertial weight value

θ made in such a way that the relationship between iteration and speed is inversely proportional. This means that as the number of iterations increases, the particle motion speed will decrease. This value varies linearly in a decreasing range of 0.9 to 0.4.

A high inertial weight value enhances global exploration, whereas a low value prioritizes local search. It is important to find an inertial weight value (θ) that balances global and local search efforts so that you don't focus too much on one aspect while also exploring new search domains within a certain dimensional space. **Equation 9** expresses the inverse correlation between inertial weights and iterations to expedite convergence.

$$\theta = \theta_{\max} - I\frac{\theta_{\max} - \theta_{\min}}{i_{\max}} \quad (9)$$

where:

$\theta_{\max}$ and $\theta_{\min}$ the maximum value and minimum value of the inertia weight, usually used value $\theta_{\max}$ = 0,9 and $\theta_{\min}$ = 0.4,

$i_{\max}$ the maximum number of iterations used,

I – the current iteration.

Speed V_{pn}^{k+1} in **Equation (8)** consists of three parts, namely the first part is V_{pn}^k shows the previous speed of the particle. The second part $b \times rand1(b)$ shows the process of completion of individual experiences. Next is the third part $c \times rand1(c)$ which shows the process of completion of the experiences of other particles, which represents various information and social cooperation between particles.

3.4. Inversion modelling

Inversion modelling is a method for enhancing geophysical modelling by extracting model parameters from observational data using inversion theory. Simultaneously, the inversion process is a mathematical procedure for estimating a model parameter from the desired model, utilising data, the original model, and the function of the model parameters. We employ three-dimensional inversion modelling to characterise subsurface conditions. Three-dimensional modelling is deemed more rational than two-dimensional modelling as it more accurately represents the geometric model in relation to the subsurface image. We conducted the modelling of the subsurface structure using a three-dimensional (3D) inversion technique. Grablox 1.6 software processed the residual anomaly gravity data to generate a three-dimensional cross-sectional density model. Either a 2D or 3D cross-section can display the resultant 3D model. The Grablox 1.6 program (**Pirttijarvi, 2008**) sequentially executes two inversion techniques: Singular Value Decomposition (SVD) inversion (base, density, heights) and Occam inversion (occam d and occam h) (see **Figure 6**) (**Hjelt, 1992**).

In **Figure 6**, you can see the shapes of the calculated and differential results for base, density, and heights from the inversion process using the Singular Value Decomposition (SVD) method and Occam method. The initial phase is base inversion. We determined the data

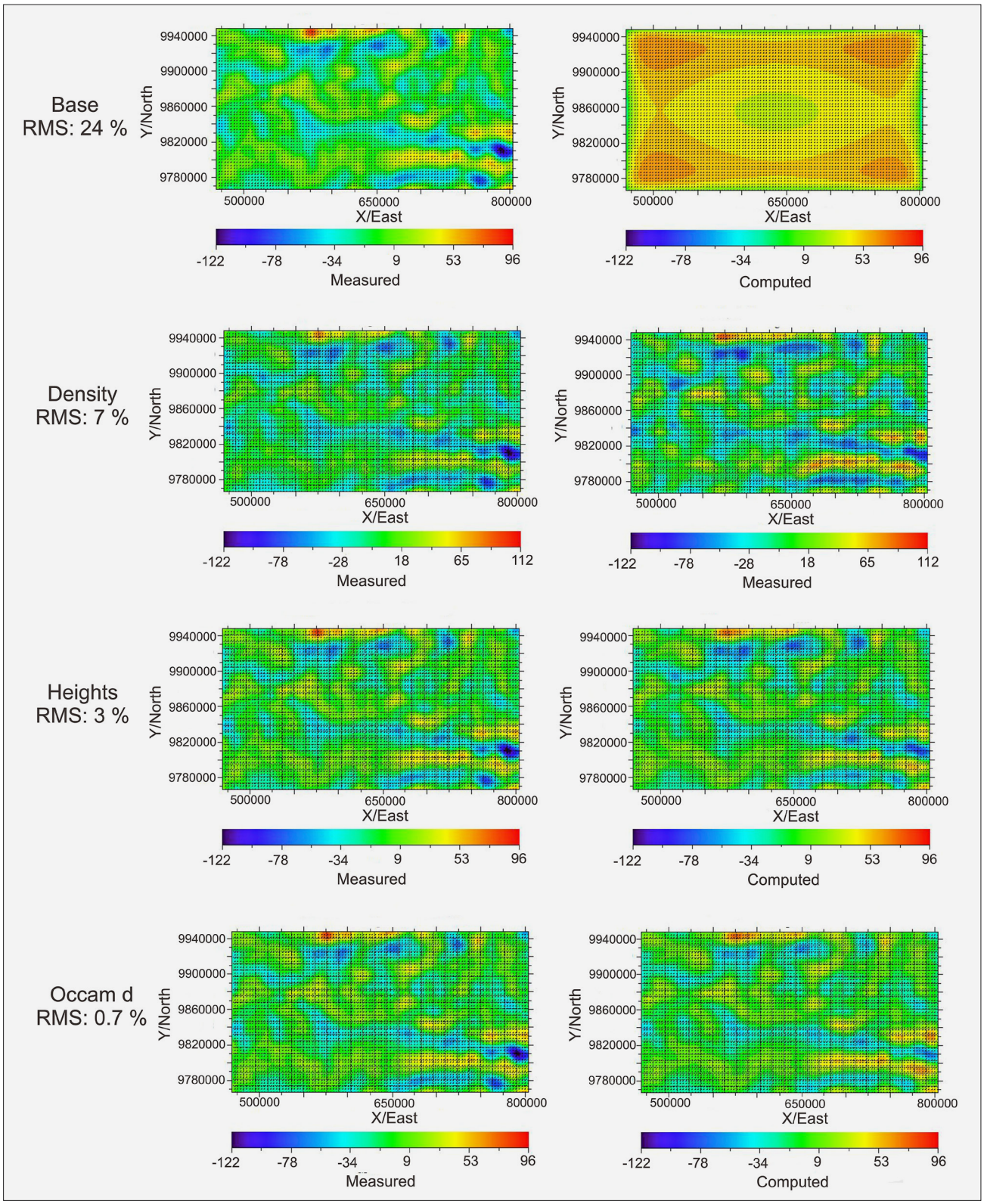

Figure 6: Inversion results in 3D modelling with Grablox

error rate at this stage of calculation to be 24%, which indicates the error rate in the fundamental parameters of anomalies or constraints post-optimisation. The contour of the base optimisation results, both computed and measured, illustrates this, with the contour pattern not yet exhibiting a correspondence between the inversion results and observations. The next step is to optimize the density, which is based on the results of density inversion calculations with a 7% error rate in the density data. However, the calculated contour is already close to the

measured contour of the study region. The subsequent step is height optimisation to refine the block's thickness. The height inversion calculations indicate that the data error rate has diminished to 3%, and the contour computation outputs are beginning to align with the observed contour pattern.

4. Results and discussion

We used the GM-SYS to calculate and corrects topography-related impacts along the two-dimensional model plane throughout the modelling process. GM-SYS is part of Geosoft Oasis Montaj software. The modeling generated the variables *x, z*, and *g*. We applied the PSO algorithm to each gravity anomaly profile (residual) to calculate the fault parameters (*x, z*, and *g*). This study processed 2D gravity data using inversion, rectified, and optimised the data using the PSO method. As an example, PSO optimisation improved 2D understanding of data processing results by focusing on the minimum RMS value (see **Figure 7**). The PSO processing in this study was based on a residual map that makes nine vertical profile incisions (see **Figure 5**). The nine profile incisions extend perpendicularly from south to north across the Sula and Balantak faults, designated as A-A', B-B', C-C', D-D', E-E', F-F', G-G', H-H', and I-I'. We used a contrast density value of roughly $\Delta\rho$ = -590 g/cm³. PSO then delineated and quantified the basement depth at each profile incision inside the fault zone region (see **Table 2**).

Figure 7 shows the 2D modelling of basement topography at each profile incision. The top image, in the form of red dots, is data from gravity anomalies, which is the main data for calculating basement depth using PSO. The dotted line represents the search bound or search limit, which is used to find the optimal depth calculation (top model) when PSO calculates basement depth (see **Table 1**). This search bound comprises two areas, representing the upper and lower limits of the search limit for the optimal model (best model). Meanwhile, the blue line is the best search result or model produced by PSO. This optimal model (best model) is derived from the calculation of the actual basement depth in this study. The PSO calculation yields the best model in the equivalent area. In this study, the equivalent area was 10% of the visible topography. The curve model that looks up and down shows a contrast in rock density, which indicates the presence of a fault. Meanwhile, the curly curve indicates the area is or is close to the subsoil.

The gravity inversion results indicate that the basement depth in the nine profile incision zones, which are perpendicular to the fault zone, range from 120 m to 9308 m. The results of the gravity inversion study depicted in **Figure 7** demonstrate the efficacy of the PSO technique in accurately recovering the true model depth. This is evidenced by the comparatively minor error or misfit value of processing (<1 mGal). To ascertain the lithology associated with the density of the region's rocks, 3D inversion modelling is required. The inversion computation, using the Singular Value Decomposition (SVD) method and the occam approach in Grablox, derives the contour for the inversion process. We analysed the final 3D inversion model using the Bloxer tool (the part of Grablox) (see **Figure 8**).

The geological formations in the research zone exhibit elevated rock density in the southern region of Taliabu Island and the northern sector of the Molucca Sea. This high-density rock originates from the marine crust and possesses a density over 2.8 g/cm³. This region exhibits a significant Bouguer anomaly value. The elevated anomaly value results from the existence of ancient, dense, thick, and rigid rock strata, leading to a greater mass density in comparison to younger and less compact rock layers. The thickness of the rock layer results from the subduction of the Australian continent beneath the Banda Sea plate, leading to the formation of substantial oceanic and continental crust above the upper mantle (**Saultan and Subagio, 2014**).

In 3D inversion modelling, the incision is the same as that utilised in PSO analysis and derivative analysis. This is conducted to ascertain the density of rocks situated inside the density contact boundary area that has been studied derivatively. The density contact limit indicates the fault's position. We compared the derivative analysis results with the Grablox modelling profile section to determine the density of rocks in the fault zone, as shown in **Figure 9**.

The results of the derivative analysis provide information regarding the existence of fault zones, as shown in **Figure 10**.

We have separated this research area into two fault zones based on derivative analysis and low residual anomaly readings. We selected the low anomaly residue because it is associated with a fault area characterized by high gravity anomaly values close to low gravity anomaly values. Fault zone 1 is where low-value residual gravity anomalies can be found on profiles A-A', B-B', C-C', D-D', E-E', F-F', G-G', H-H', and I-I'. The baseline depth ranges from 2843.3 m in the B-B' incision profile to 6526.9 m in the H-H' incision profile. Meanwhile, the geological structure revealed from the area's 3D Grablox modeling study consists of constituent rocks with low-density values ranging from 1.68 gr/cm³ to 2.20 gr/cm³. Meanwhile, the southern section of fault zone 1 contains high-density rock with a density of 3.2 g/cm³. Fault zone 2 intersects the minimum residual gravity anomaly along the incision profiles A-A', B-B', C-C', D-D', E-E', F-F', G-G', H-H', and I-I'. The B-B' profile has the shallowest basement depth, measuring 3716.3 m, while the I-I' profile has the deepest, measuring 9308.4 m. The geological structure revealed by the 3D Grablox modeling investigation indicates that the area has rock elements with a low density of 1.24 g/cm³. The northern region of fault zone 2 consists of rocks with an average density of 2.4 g/cm³. Concurrently, the

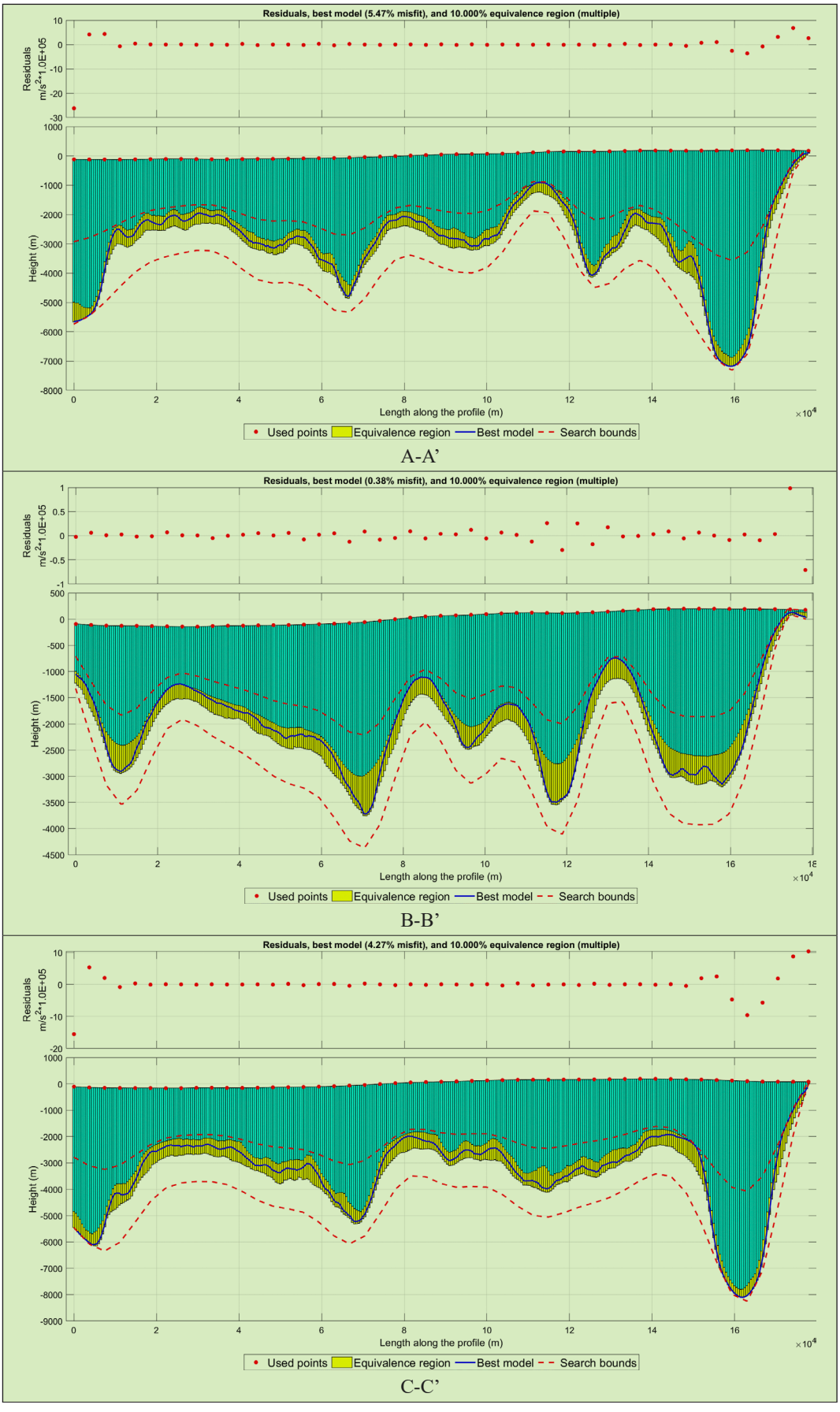

Figure 7: PSO conducted the inversion analysis, using basement depth data at each profile incision

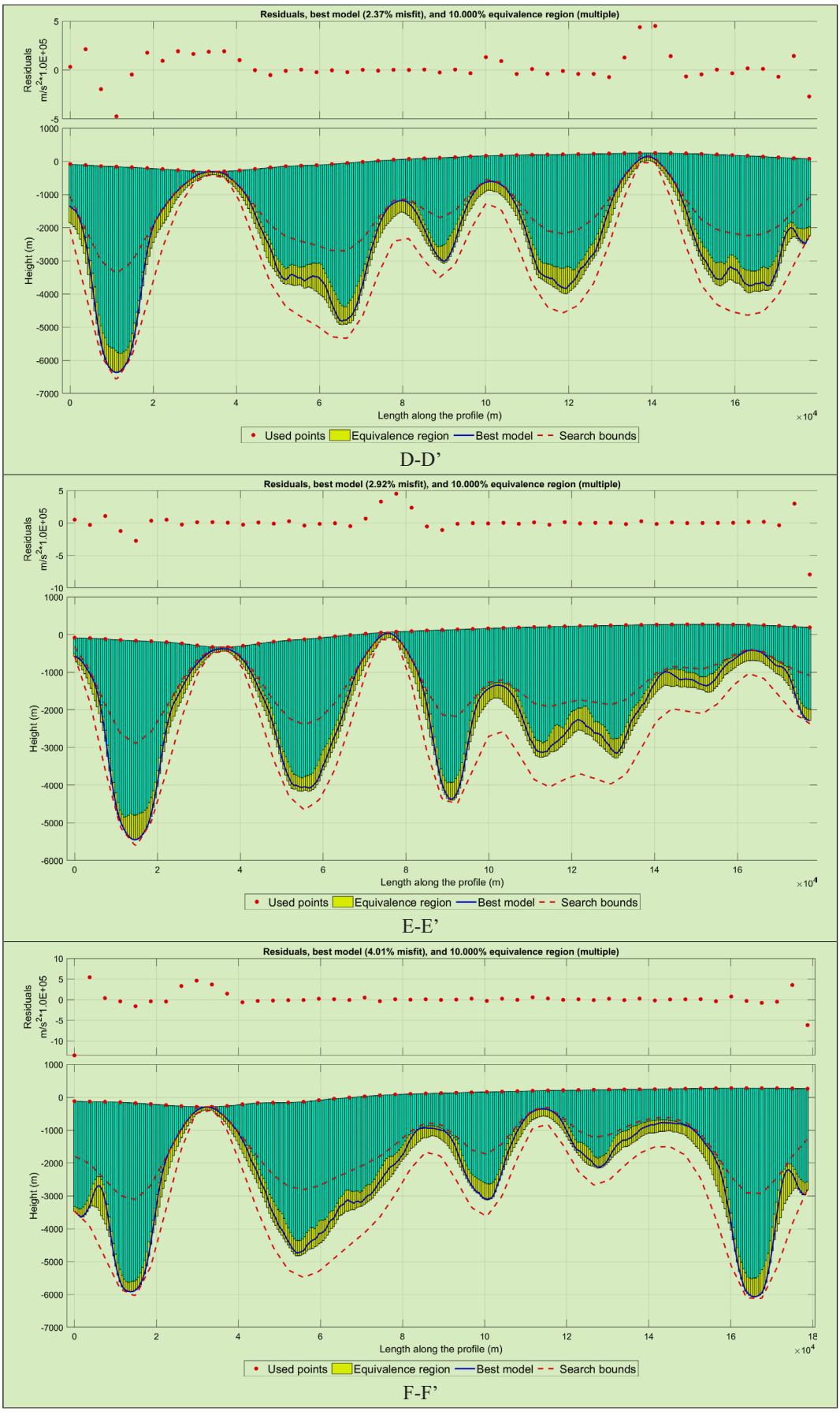

Figure 7: Continued

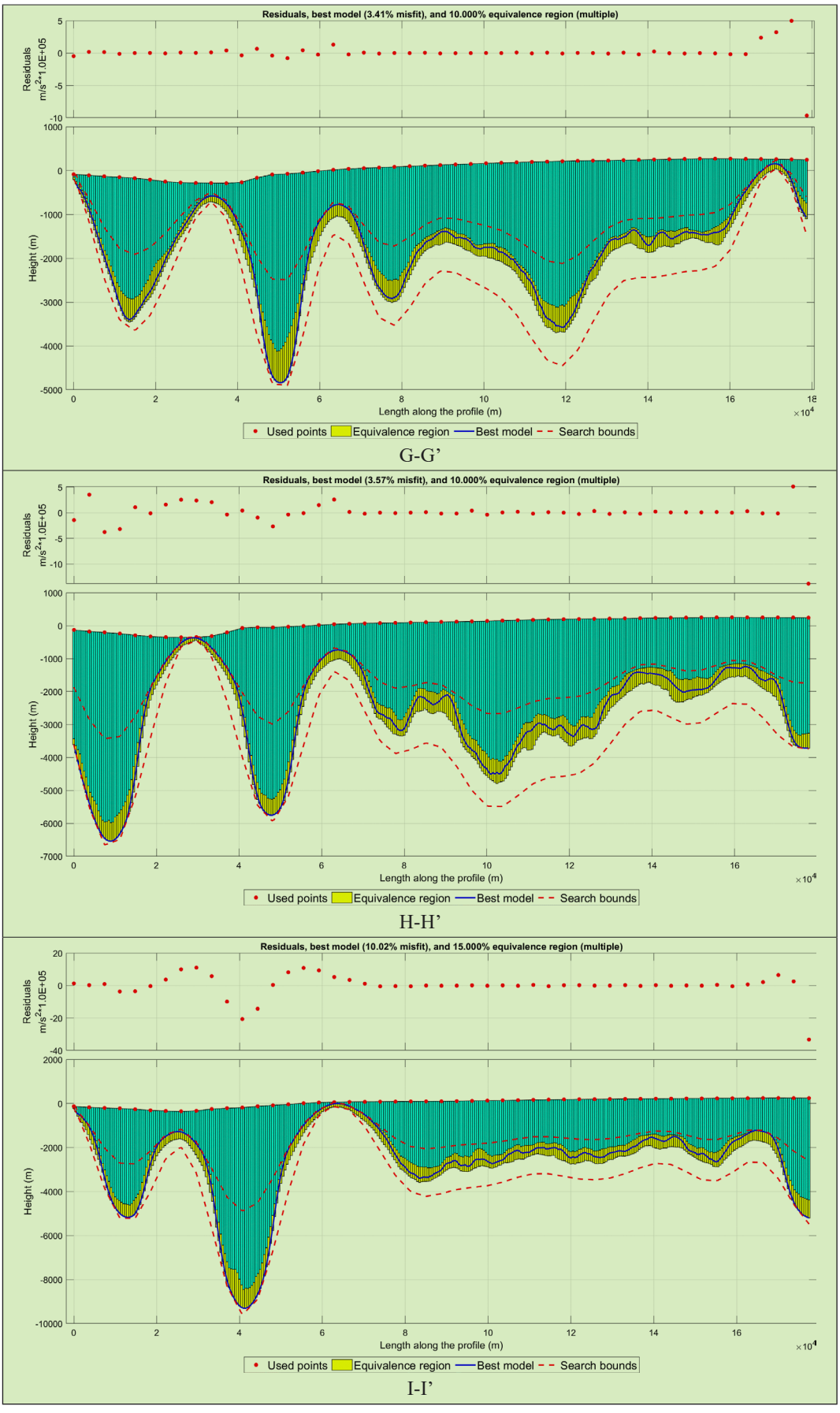

Figure 7: Continued

Table 1: Predicted basement geometric parameters, including depth ranges and average depth

Incision	Number Profile	Gravity Anomaly Missfit (mGal)	Depth (m)	The Average Depth (m)
A-A'	356	0.0251	7178.1	2959.8
B-B'	357	0.0038	3716.3	1994.2
C-C'	356	0.0427	8098.3	3410.2
D-D'	356	0.0237	6366.9	2382.2
E-E'	355	0.0292	5450.4	1992.9
F-F'	356	0.0401	6069.9	2407.9
G-G'	357	0.0341	4839.4	1819.6
H-H'	356	0.0571	6543.5	2675.1
I-I'	355	0.1002	9308.4	2676.9

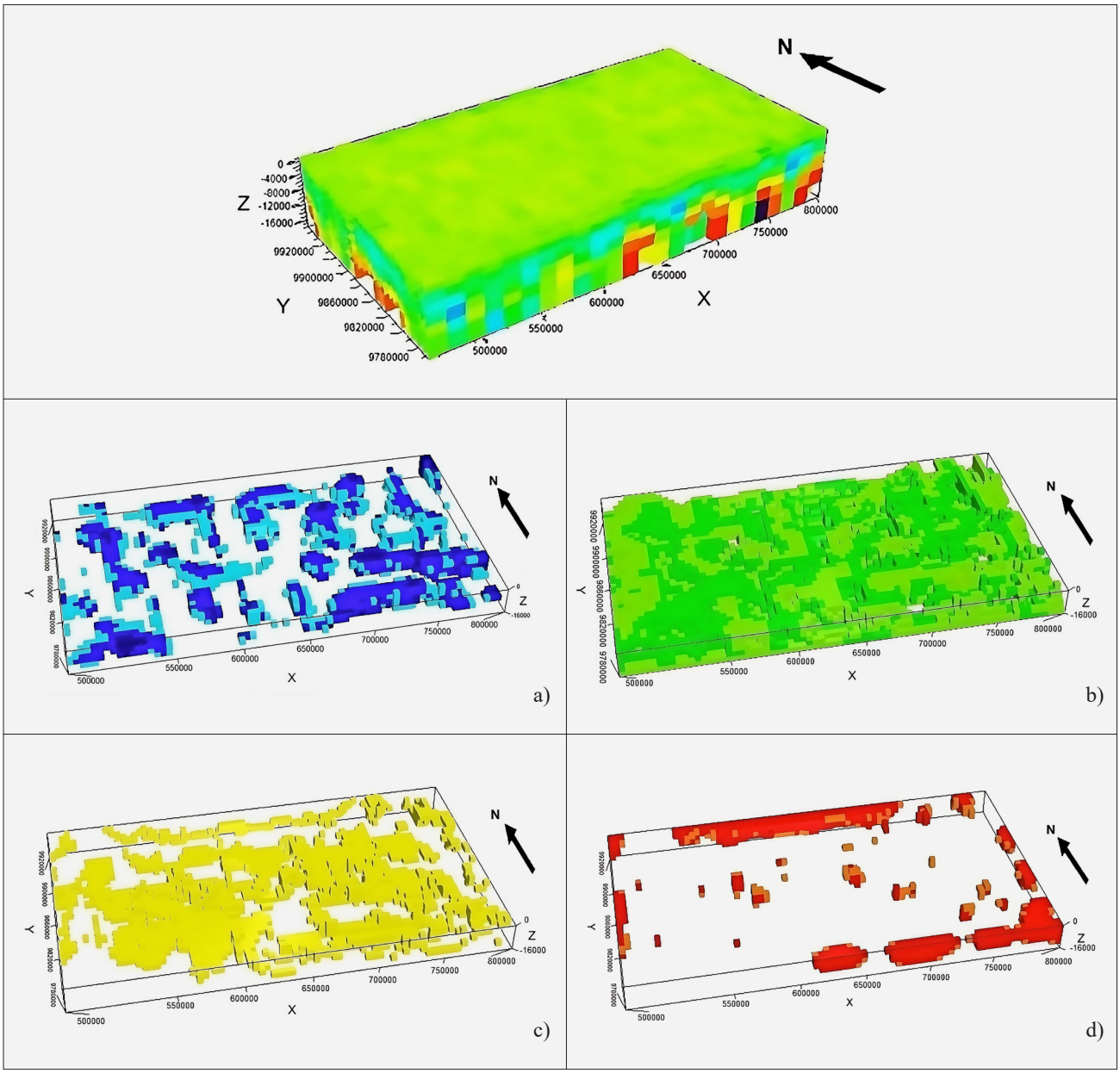

Figure 8: Density of the rocks that make up the research area in inversion modelling results using Grablox software. a) Density < 2.3 g/cm³. b) Density 2.31 g/cm³ – 2,64 g/cm³. c) Density 2.65- 2.78 g/cm³. d) Density > 2.8 g/cm³.

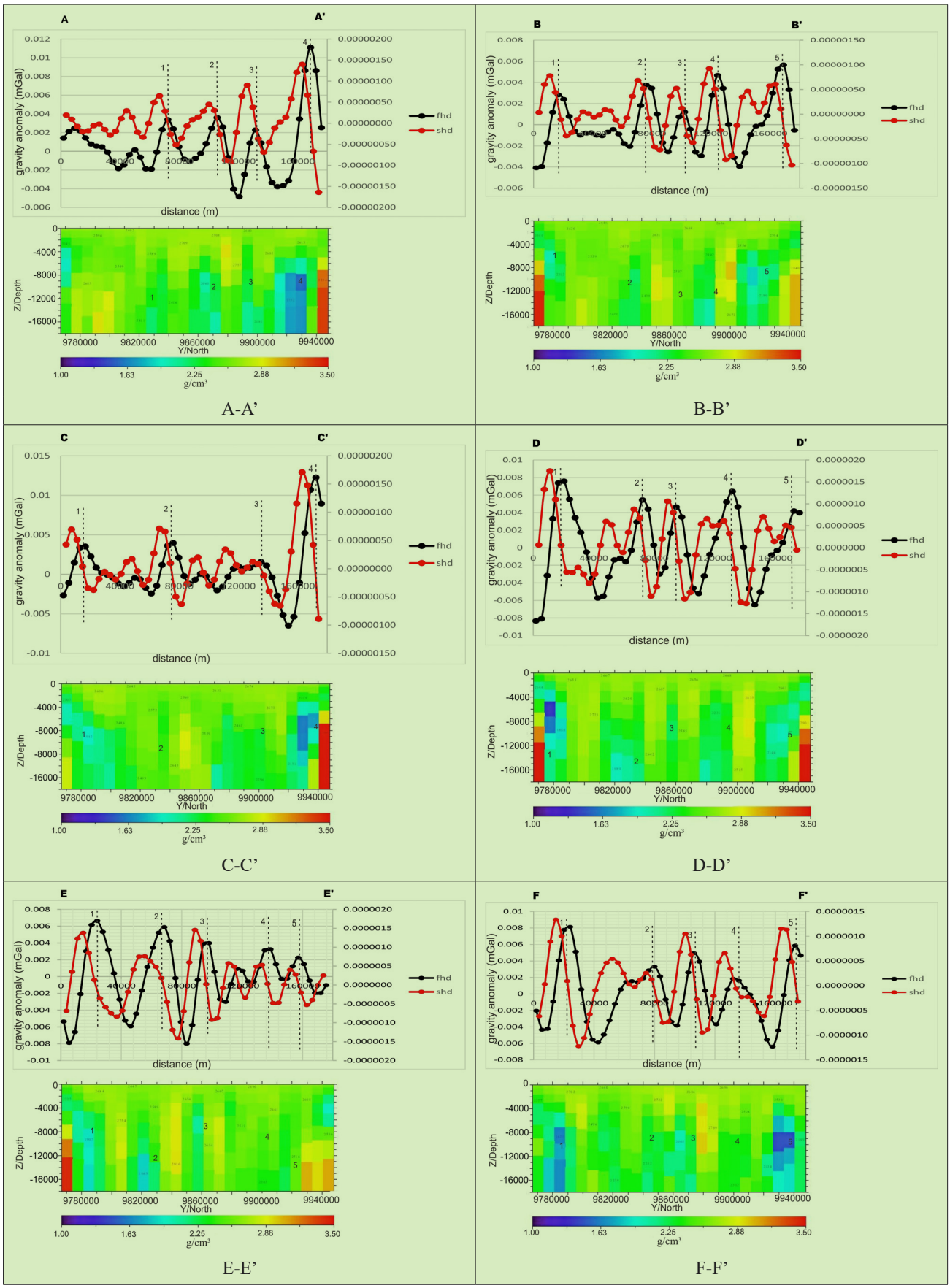

Figure 9: The process of identifying the density contrast boundary site, which signifies the occurrence of faults, involves using derivative analysis (top) and adjusting it to the A-A' to I-I' profile incision in 3D modelling (bottom).

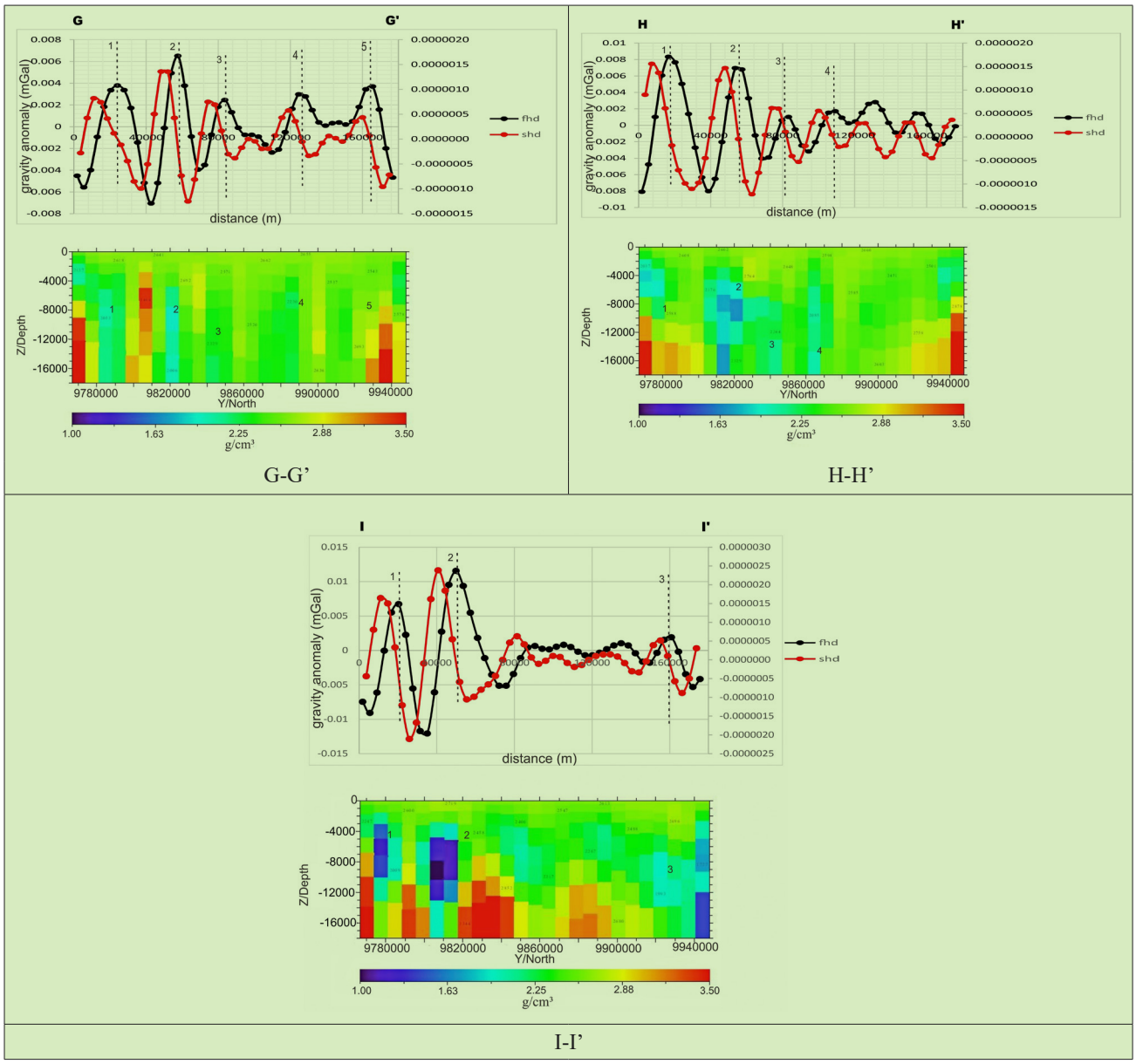

Figure 9: Continued

southern region of the profile incision has rocks with an average density ranging from 2.5 g/cm³ to 2.7 g/cm³. The average depth of faults in fault zones 1 and 2 is 5200 m. **Table 2** presents the anticipated basement depth data for fault zones 1 and 2 throughout each profile section.

The inversion approach utilising Particle Swarm Optimisation can provide estimations for the basement depth of the fault zone. Derivative analysis reveals that the east-west-trending fault structure in fault zone 1 and fault zone 2 corresponds with the tectonic features of the Banggai-Sula microcontinent, thereby confirming the existence of an east-west fault in the region (see **Figure 10**). The outcomes of this approach may yield significant insight for the continued examination of fault zones, particularly in studies of structural geometry.

5. Conclusions

The distribution of residual gravity anomalies in the study area exhibits values ranging from -48.8 mGal to 38.6 mGal. The range of low residual anomalies extends from -48.8 mGal to -2.3 mGal. The distribution of low anomalies aligns with the geological configuration of faults. Concurrently, significant anomalies, specifically ranging from 8.3 mGal to 38.6 mGal, indicate elevated rock density. Gravity inversion using PSO revealed that the fault zone's basement depth ranged from 120 to 9308 m. The basement depths of the fault zone 1 are from 2843.3 m to 6526.9 m. In addition, the Grablox 3D modeling study reveals geological layers with rock elements ranging in density from 1.68 g/cm³ to 2.20 g/cm³, while

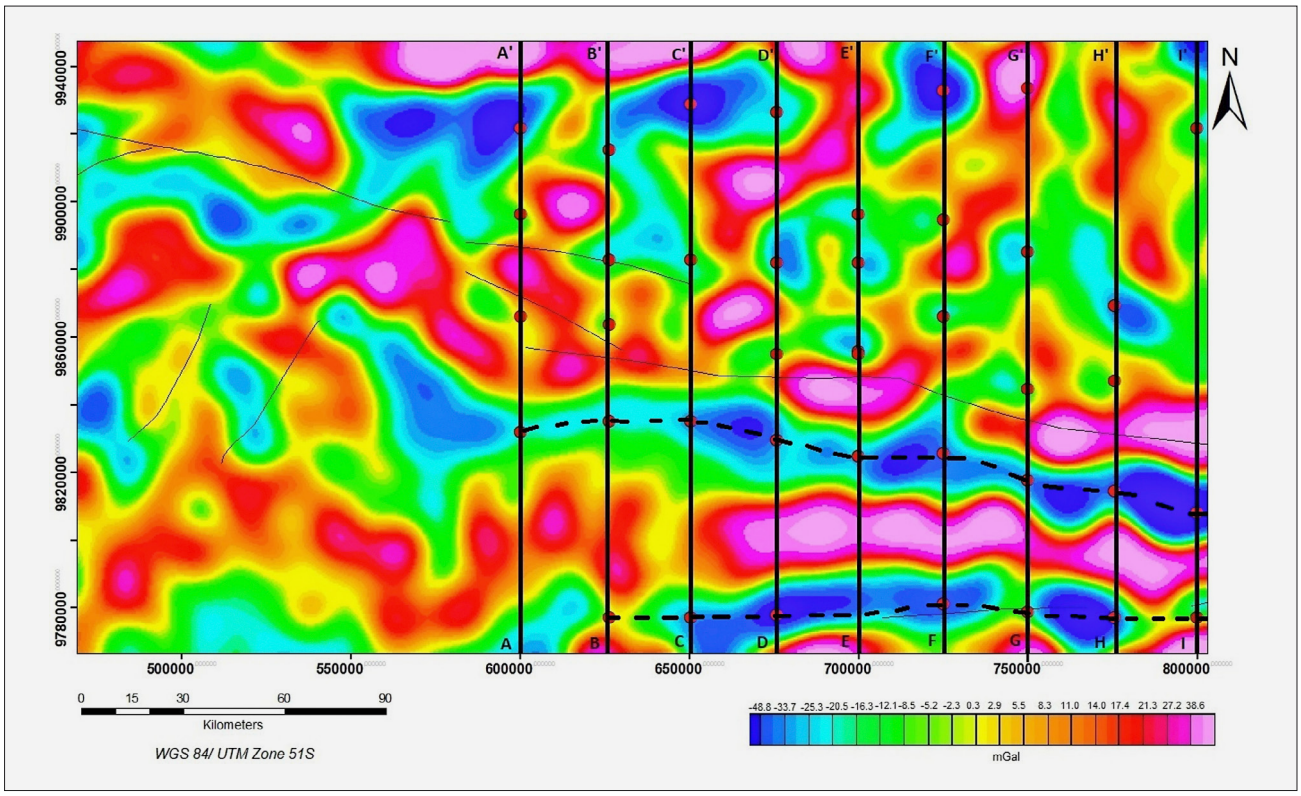

Figure 10: The density contrast border, represented by a red circle, signifies the presence of a fault based on derivative analysis, while the division of fault zones is based on low residual anomaly values.

Table 2: Predicted basement depth at each profile section of fault zones 1 and 2

Area	A-A' (m)	B-B' (m)	C-C'(m)	D-D' (m)	E-E' (m)	F-F' (m)	G-G' (m)	H-H' (m)	I-I' (m)
1	5263.8	2843.3	6200.7	6366.9	5442.8	5951.8	3400.3	6526.9	5164.8
2	4532.9	3716.3	5460.4	4905.6	4253.1	4617.1	4816.6	5786.8	9308.4

south of this Fault Zone 1, the high-density rock is 3.2 g/cm^3. The Fault Zone 2, which intersects the lowest residual gravity anomaly value in the same nine incision profiles, has basement depth ranges of 3716.3 m and 9308.4 m, respectively. Rocks with a low-density value of 1.24 g/cm^3 are part of the geological structure this zone. In the north of the fault zone 2, rocks have an average density value of 2.4 g/cm^3, and in its south, rocks have an average density of 2.5 g/cm^3 to 2.7 g/cm^3. The average depth of faults in fault zones 1 and 2 is 5200 m. The inversion method using PSO can yield estimates for the basement depth of the fault zone. Derivative analysis indicates that the east-west-trending fault structure in fault zone 1 and fault zone 2 aligns with the tectonic characteristics of the Banggai-Sula microcontinent, hence affirming the presence of an east-west fault in the area.

Acknowledgement

There were no conflicts of interest in the development of this book. The author is grateful to the reviewer of this paper and the National Research and Innovation Agency (BRIN) for sponsoring a Degree by Research scholarship program to help them successfully complete their studies.

6. References

Alqahtani, F., Abraham, E. M., Aboud, E., and Rajab, M. (2022): Two-Dimensional Gravity Inversion of Basement Relief for Geothermal Energy Potentials at the Harrat Rahat Volcanic Field, Saudi Arabia, Using Particle Swarm Optimisation. Energies, 15(8). https://doi.org/10.3390/en15082887.

Beaudouin, T., Bellier, O. & Sebrier, M. 2003. Present-day stress and deformation fields within the Sulawesi Island area (Indonesia): geodynamic implications. Bulletin de la Société géologique de France, 174, 305–317.

Blakely, R. J. (1996): Potential Theory in Gravity and Magnetic. In Cambridge University Press.

Chakravarthi, V., Sundararajan, N. (2005): Gravity modeling of 2.5D sedimentary basins with 199 density contrast varying with depth. Computer and Geosciences. 31, 820-827.

Chapell, A., and Kusznir, N. (2008): An algorithm to calculate the gravity anomaly of sedimentary basins with exponential density–depth relationships. Geophys. Prospect. 56, 249– 258.

Cordell, L. (1973): Gravity analysis using an exponential density-depth function—San Jacinto Graben, California. Geophysics 38 (4), 684–690.

Eberhart, R. and Kennedy, J. (1995): A new optimizer using particle swarm theory. In MHS'95. Proceedings of the Sixth International Symposium on Micro Machine and Human Science, 39–43.

Ferdian, F., Hall, R., and Watkinson, I. (2011): A Structural Re-Evaluation of the North Banggai-Sula Area, Eastern Indonesia. Proceedings, Indonesian Petroleum Association Thirty-Fourth Annual Convention & Exhibition.1-20.

Garrard, R., Supandjono, J. B., and Surono. (1988): The Geology of the Banggai-Sula Microcontinent, Eastern Indonesia. In: Proceedings Indonesian Petroleum Association, 17th Annual Convention, 23–52.

Gunawan, B., Anjani, A., and Anjalni, A. (2022): Identification of 2D Modelling and Surface Temperature of the Mount Gede-Pangrango Geothermal Area, West Java using the Gravity Method. Journal of Engineering Environtmental Energy and Science. 1(1), 1-14.

Granser, H. (1987): Three-dimensional interpretation of gravity data from sedimentary basins using an exponential density-depth function. Geophysical Prospecting, 35(9), 1030–1041.

Hall, R. (2002): Cenozoic geological and plate tectonic evolution of SE Asia and the SW Pacific: Computer-based reconstructions, model and animations. Journal of Asian Earth Sciences, 20, 353–431.

Hamilton, W. (1979): Tectonics of the Indonesian Region. Bulletin of the Geological Society of Malaysia, 6, 3–10.

Lillie, R. J. (1999): Whole Earth Geophysics: An Introductory Textbook for Geologists and Gophysicists. In Oregon State University. Prentice-Hall, Inc., United States of America.

Maulana, A. D., Prasetyo, D. A., and Setiawan, A. F. (2021): Mathematical Analysis of Determining the New Bouguer Correction Constant on Topex Satellite Gravity in the Implications of Geological Conditions, Case Study of the Palu Koro Fault, Central Sulawesi. Journal of Applied Geoscience, 3(1), 10.

McCaffrey, R., Silver, E., and Raitt, R. (1980): Crustal Structure of the Molucca Sea Collision Zone, Indonesia. In The tectonic and geologic evolution of Southeast Asian seas and islands. Part 1, 161–177.

Moore, G. F. & Silver, E. A. (1980): Collision Processes in the Northern Molucca Sea. In: Hayes, D. E. (ed.) The Tectonic and Geologic Evolution of Southeast Asian Seas and Islands. American Geophysical Union, Geophysical Monograph, 27, 360–372.

Pallero, J. L. G., Fernández-Martínez, J. L., Bonvalot, S., and Fudym, O. (2015): Gravity inversion and uncertainty assessment of basement relief via Particle Swarm Optimisation. Journal of Applied Geophysics, 116, 180–191.

Pallero, J. L. G., Fernández-Martínez, J. L., Fernández-Muñiz, Z., Bonvalot, S., Gabalda, G., & Nalpas, T. (2021): GRAVPSO2D: A Matlab package for 2D gravity inversion in sedimentary basins using the Particle Swarm Optimization algorithm. Computers and Geosciences, 146, 1–56.

Pigram, C. J., and Supandjono, J. B. (1985): Origin of the Sula Platform, eastern Indonesia. Geology, 13(4), 246–248.

Pirttijarvi, M. (2008): Gravity Interpretation and Modelling Software Based on a 3- D Block Model. User Guide: University of Oulu.

PuSGeN. (2017): Peta Sumber dan Bahaya Gempa Indonesia 2017. In Pusat Penelitian dan Pengembangan Perumahan dan Permukiman, Badan Penelitian dan Pengembangan, Kementerian Pekerjaan Umum dan Perumahan Rakyat, Bandung, 376p.

Rao, D.B. (1990): Analysis of gravity anomalies of sedimentary basins by an asymmetrical trapezoidal model with quadratic density function. Geophysics, 55(2):226–231.

Rosid, M. S., and Siregar, H. (2017): Determining Fault Structure Using First Horizontal Derivative (FHD) and Horizontal Vertical Diagonal Maxima (HVDM) Method. AIP Conference Proceedings, Vol. 1862.

Roy, A., Dubey, C. P. and Prasad, M. (2021): Gravity inversion for heterogeneous sedimentary basin with b-spline polynomial approximation using differential evolution algorithm. Geophysics, 86, 1–63.

Saultan, P., and Subagio. (2014): Gravity Anomaly Patterns in the Taliabu-Mangole Area and the Surrounding Seas are Related to the Petroleum and Gas Prospects. Journal of Marine Geology, 12(2), 65–78.

Setiadi, I., Widodo, J., and Nainggolan, T. B. (2021): Geological interpretation of offshore Central Sumatra basin using topex satellite gravity data. IOP Conference Series: Earth and Environmental Science, 944(1).

Silver, E., Mccaffrey, R., Joyodiwiryo, Y., and Stevens, S. (1983): Ophiolite emplacement by collision between the Sula Platform and the Sulawesi Island Arc, Indonesia. Journal of Geophysical Research, 88, 9419–9436.

Smith, W. H. F., and D. T. Sandwell. (1997): Global seafloor topography from satellite altimetry and ship depth soundings, Science, v. 277, p. 1957-1962.

Supandjono, B., and E. Haryono. (1993): Peta Geologi Lembar Banggai, Sulawesi-Maluku (Skala1: 250.000). Bandung.

Surono and Sukarna (1993): Peta Geologi Lembar Sanana, Maluku (Skala 1: 250.000). Bandung.

Surono (2012): Tectonostratigraphy of the eastern part of Sulawesi, Indonesia. in relation to the terrane origins. Journal of Geology and Mineral Resources, 22(4), 199–207.

Watkinson, I. M., Hall, R., and Ferdian, F. (2011): Tectonic re-interpretation of the Banggai Sula-Molucca Sea margin, Indonesia. Geological Society Special Publication, 355, 203– 224.

Zakaria, Z., and Sidarto, D. (2015): Tectonic activity in Sulawesi and its surroundings from the Mesozoic to the present as a result of the interaction of the tectonic activity of the major tectonic plates in the surrounding area. Journal of Geology and Mineral Resources, 16(3), 115–127.

Zhang, S., Sandwell, D. T., Jin, T., and Li, D. (2017): Inversion of marine gravity anomalies over southeastern China seas from multi-satellite altimeter vertical deflections. Journal of Applied Geophysics, 137, 128–137.

SAŽETAK

Identificiranje temeljne strukture rasjedne zone Sula u regiji mikrokontinenta Banggai-Sula, Molučko more, na temelju 2D modeliranja gravitacijske inverzije korištenjem optimizacije roja čestica i 3D modeliranja korištenjem Grabloxa

Cilj je ove studije odrediti temeljnu strukturu rasjednih zona Sula unutar regije mikrokontinenta Banggai-Sula implementacijom 2D i 3D modeliranja gravitacijske inverzije. Rasjed Sula rezultat je konvergencije između mikrokontinenta Banggai-Sula i sjevernih regija ili kompresije uzrokovane ekstruzijom materijala iz zone kolizije Molučkoga mora prema jugu. To je aktivan rasjed s nekoliko potresa u posljednja dva desetljeća. Budući da je riječ o složenome aktivnom rasjedu, postoje neke nepoznanice, posebice u strukturi rasjeda. Podatci o rezidualnim anomalijama modelirani su dvodimenzionalno pomoću metode optimizacije roja čestica i trodimenzionalno pomoću softvera Grablox. Rezultati gravitacijske inverzije pokazuju da se dubina temeljne strukture u devet zona usjeka profila okomitih na zonu rasjeda kreće od 120 m do 9308 m. Ovo istraživačko područje može se podijeliti u dvije rasjedne zone na temelju rezidualnih anomalija niske vrijednosti. Rasjedna zona 1 pokazuje raspon dubina temeljne strukture od 2843,3 m do 6526,9 m. Ovo područje ima komponente stijena niske gustoće u rasponu od 1,68 g/cm^3 do 2,20 g/cm^3. Rasjedna zona 2 pokazuje raspon dubina temeljne strukture od 3716,3 m do 9308,4 m. Geološki sloj sastoji se od konstitutivnih stijena s niskom gustoćom od 1,24 g/cm^3, za razliku od sjevernih stijena koje imaju prosjek od 2,4 g/cm^3 i južnih stijena s prosjekom između 2,5 g/cm^3 i 2,7 g/cm^3. Prosječna dubina rasjeda u rasjednoj zoni 1 i 2 iznosi 5200 m. Metoda inverzije koja primjenjuje PSO može dati procjene za dubinu temeljne strukture zone rasjeda. Izvedena analiza pokazuje da je rasjedna struktura usmjerena istok-zapad u rasjednoj zoni 1 i rasjednoj zoni 2 usklađena s tektonskim karakteristikama mikrokontinenta Banggai-Sula, čime se potvrđuje prisutnost rasjeda istok-zapad u tome području.

Ključne riječi:
gravitacija, inverzijsko modeliranje, optimizacija roja čestica, Banggai-Sula, Molučko more

Author's contribution

Cahya Damayanti (PhD Candidate, Geophysics) handled data collection, processing, and writing the paper. **Sismanto Sismanto** (Professor, Exploration Geophysics and Seismology), contributed to the paper's review and comprehensive drafting. **Ari Setiawan** (PhD, Geophysics and Geodynamics) contributed to the theoretical concept of the study. **Lina Handayani** (PhD, Geophysics) helped to write the study.